energies

MDPI

Article

Robust Frequency Regulation of Hybrid Wind–PV Thermal Power Systems via Adaptive Fractional-Order PID Control

Yevgeniy Muralev [1], Dinmukhambet Baimbetov [1,*], Samal Syrlybekkyzy [1], Mohamed Salem [2,3,4,*], Ali Bughneda [5] and Khalid Yahya [6,*]

[1] Faculty of Engineering, Yessenov University, 32nd District, 1, Aktau 130000, Kazakhstan; yevgeniy.muralev@yu.edu.kz (Y.M.); samal.syrlybekkyzy@yu.edu.kz (S.S.)
[2] Institute of Research and Development, Duy Tan University, Da Nang 550000, Vietnam
[3] School of Engineering & Technology, Duy Tan University, Da Nang 550000, Vietnam
[4] Libyan Authority for Scientific Research, Tripoli P.O. Box 80045, Libya
[5] Department of Electrical and Electronic Engineering, College of Technical Sciences-Bani Walid, Bani Walid P.O. Box 38645, Libya; bughneda@ctsbw.edu.ly
[6] Department of Electrical & Electronics Engineering, Istanbul Gelisim University, 34310 Istanbul, Turkey
* Correspondence: dynmuhambet@gmail.com (D.B.); mohamadsalemmohamedothman@duytan.edu.vn (M.S.); hayahya@gelisim.edu.tr (K.Y.)

Abstract

As modern electrical grids increasingly incorporate renewable generation—specifically from wind and solar–thermal installations—they face heightened volatility and operational complexities, which severely complicate load frequency regulation. While fractional-order proportional-integral-derivative (FOPID) controllers are commonly employed for this purpose, their conventional formulations rely on fixed fractional parameters that cannot adapt to fluctuating network conditions. To address this limitation, the present study develops an adaptive FOPID (AFOPID) control architecture capable of real-time adjustment of fractional orders, thereby enhancing regulatory effectiveness. The Coot Optimization Algorithm (COA) is utilized to optimally determine the operational parameters of all controllers under investigation. The proposed strategy is validated on a simulated hybrid power system comprising wind generation, solar–thermal units, and physical nonlinearities including governor dead band and generation rate constraints. A comparative analysis is conducted across four distinct operating scenarios, benchmarking the COA-tuned AFOPID against conventional PI, PID, and standard FOPID controllers. Quantitative results demonstrate that the proposed COA-AFOPID configuration achieves superior performance, with improvements in settling time up to 46.06% and reductions in ITAE index up to 89.89% compared to traditional methods. These findings confirm the enhanced stability and robustness of the proposed approach for frequency regulation in sustainable energy networks.

Keywords: wind power; solar–thermal power; frequency regulation; fractional order proportional integral derivative (FOPID); adaptive controller; coot optimization algorithm

Check for updates

Academic Editor: Armando Oliveira

Received: 21 April 2026
Revised: 20 June 2026
Accepted: 24 June 2026
Published: 29 June 2026

Copyright: © 2026 by the authors. Licensee MDPI, Basel, Switzerland. This article is an open access article distributed under the terms and conditions of the Creative Commons Attribution (CC BY) license.

1. Introduction

The transition toward eco-friendly power production has made renewable energy sources indispensable to contemporary electrical grids. A primary driver for this shift is the urgent need to curtail the ecological degradation traditionally associated with carbon-intensive electricity generation. Technologies that harness sunlight, wind, water, and organic matter operate with virtually zero greenhouse gas emissions. Consequently, pivoting away from combustible resources directly aids in combating global warming and

improving atmospheric conditions. Furthermore, broadening the spectrum of generation assets bolsters grid resilience and diminishes vulnerabilities tied to foreign fuel procurement. Nevertheless, while adopting these green technologies satisfies both ecological and financial objectives, the inherent intermittency of wind velocity and solar insolation—coupled with fluctuating consumer demand—poses a severe threat to network frequency synchronization.

Renewable energy sources (RESs), such as solar and wind power, are highly dependent on weather conditions and exhibit fluctuations in their output. As a result, establishing capable regulatory frameworks is vital to suppress extreme operational deviations across modern power systems [1]. Considering the participation levels of different RESs in a power grid, the significance of appropriate system dynamics becomes evident [2]. Load frequency control (LFC) ensures the stability, reliability, and performance of power systems by mitigating the challenges associated with integrating RESs. Within contemporary electrical networks, LFC operates by continuously calibrating the generation-to-demand ratio across linked control areas, thereby sustaining operational balance despite highly variable consumption patterns [3].

The literature on LFC has explored various control strategies including robust control, adaptive control, model predictive control, fuzzy logic-based controllers, and sliding mode control (SMC) [4–6]. Recent studies have demonstrated the successful application of fuzzy controllers [7] and SMC [8] in various power system scenarios. Collectively, these studies offer thorough evaluations of both conventional and advanced control strategies. The existing body of research consistently indicates that PID-based controllers remain among the most prevalent solutions for addressing LFC issues due to their straightforward design and effortless deployment [9–11].

A comprehensive examination of existing LFC literature reveals that while PID family controllers are commonly utilized, their functionality is limited to specific operating conditions, rendering them susceptible to external disturbances. In light of these challenges, researchers have been driven to explore advanced control structures, leading to the application of fractional-order PID (FOPID) controllers. The key contribution in this area is the introduction of the fractional FOPID controller [12]. This controller involves two additional tuning parameters—namely, the derivative and integral fractional-order operators—imparting greater flexibility and robustness compared to PID controllers. The advantages of FOPID controllers have drawn considerable interest in active power system control [13–15]. For instance, a feedforward-based FOPID control strategy for microgrids has demonstrated substantial improvement in the integral time absolute error (ITAE) relative to standard PID implementations [13]. Another study confirmed the superiority of FOPID over conventional PID for frequency regulation in a four-area unbalanced power system incorporating HVDC and plug-in electric vehicles [16].

Incorporating artificial intelligence optimization frameworks into FOPID controllers for LFC has gained considerable attention. A comprehensive review by [17] examined diverse FOPID controller structures based on optimization techniques for LFC in power systems. For instance, the atom search optimization (ASO) algorithm has been utilized to tune FOPID controller parameters for LFC in an interconnected hybrid power system including plug-in electric vehicles and RESs [18]. Furthermore, a fuzzy-based non-integer PID framework using an enhanced Harris Hawks optimization (mHHO) technique has been introduced to manage grid frequency [1]. Several other optimization techniques have been successfully applied for tuning FOPID controller parameters, including the quasi-oppositional JAYA (QOJAYA) [19] and the crow search algorithm (CSA) [20].

Table 1 summarizes the most relevant previous studies on LFC systems and FOPID controllers, highlighting their methodologies, limitations, and key findings.

Table 1. Summary of previous studies on LFC and FOPID controllers.

Reference	Control Strategy	Optimization Method	Key Findings	Limitations
[1]	Fuzzy fractional-order PID	mHHO	Enhanced frequency regulation	Fixed fractional parameters
[7]	Self-tuning Fuzzy-PI	None	Effective with wind energy	Integer-order only
[13]	Feedforward FOPID	Harmony search	Improved ITAE in microgrids	Fixed λ and μ
[16]	FOPID with HVDC	None	Outperformed PID	Offline tuning
[18]	FOPID	ASO	Superior in hybrid systems	No adaptability
[19]	2-DOF PID	QOJAYA	Improved AGC performance	Integer-order
[20]	Fuzzy PID	Adaptive crow search	Good for AGC systems	Not fractional-order

Most articles treat FOPID controller parameters as fixed constants after offline tuning. Given the expanding scale of power systems and increased integration of RESs, adopting adaptive control structures is considered a viable approach for LFC, as they can accommodate uncertainties in power systems with high renewable energy penetration [21].

To address the identified research gaps, the present study introduces an adaptive FOPID (AFOPID) controller, termed the COA-AFOPID controller, which integrates an adaptive strategy, FOPID control, and the Coot Optimization Algorithm (COA) [22]. The standard FOPID architecture is upgraded via a self-tuning mechanism that continuously modifies the non-integer integration and differentiation parameters using a non-linear hyperbolic secant function (HSF) [23]. The COA [22] is utilized to fine-tune controller parameters, enhancing control performance in dynamic power systems with RES penetration.

The primary contributions of this work are: (1) development of an adaptive FOPID controller with real-time adjustment of λ and μ using HSF, (2) application of COA for optimal parameter tuning, (3) comprehensive validation on a two-region hybrid grid with thermal, wind, solar–thermal, electrolyzers, and fuel cells considering generation rate constraints (GRCs) and governor dead band (GDB), and (4) quantitative benchmarking against PI, PID, and FOPID controllers.

The remainder of this manuscript is organized as follows: Section 2 details the hybrid power network architecture. Section 3 outlines the COA methodology. Section 4 presents the COA-AFOPID regulatory mechanism. Section 5 presents simulation results across four scenarios. Section 6 presents concluding remarks.

2. The System Under Study

This study explores a multi-zone grid, illustrated in Figure 1, which consists of several interconnected zones. The grid incorporates different components, including a thermal power plant, as well as RESs like solar–thermal and wind farms. It also integrates fuel cells, electrolyzers, and PEVs. It is emphasized that the nonlinear physical constraints, including GRC and GDB were explicitly incorporated into the thermal power plant model. These constraints are critical for realistic LFC analysis, as they significantly affect system dynamics and controller performance. The specific parameters of this grid have been defined in previous works conducted by [14,18,24,25].

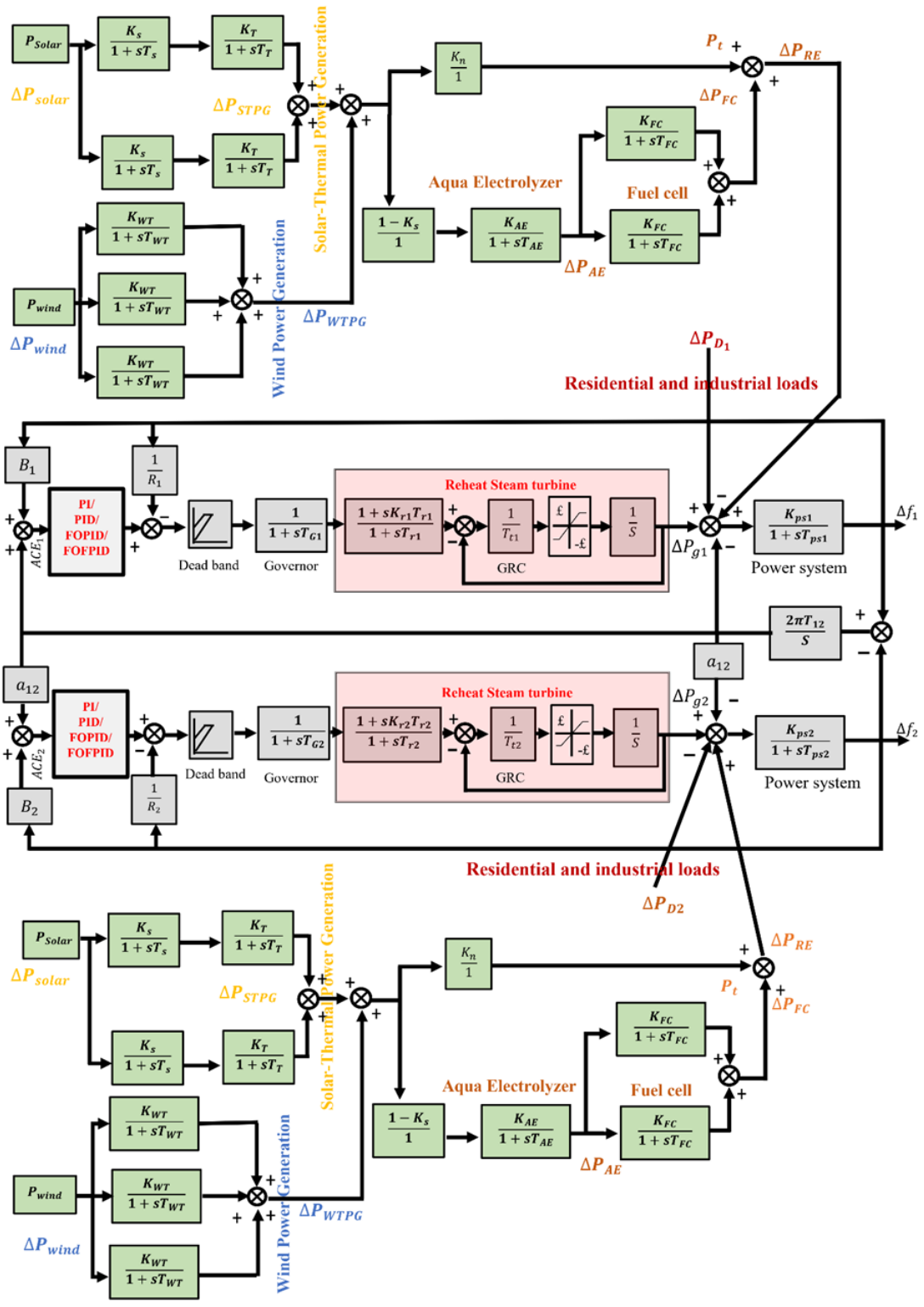


Figure 1. The System Under Study.

2.1. The Mathematical Model of Wind Generation

Among renewable energy technologies, wind power has shown the highest growth rate in recent years. It contributes to sustainable electricity generation by eliminating direct pollutant emissions. In addition, wind energy systems typically have relatively low operational and maintenance costs compared to other renewable sources [26]. However, when integrating wind energy into the power grid, there can be fluctuations in frequency because of the unpredictable nature of wind power generation [18,27]. To maintain a

stable power balance, energy storage systems like electrolyzers and fuel cells are used in combination with wind turbines (WTs). In this study, the integration of wind turbines (WTs) into the hybrid power system is modeled using a first-order transfer function, as given in Equation (1).

$$G_{WT}(s) = \frac{K_{WT}}{1 + sT_{WT}} = \frac{\Delta P_{WTPG}}{\Delta P_{wind}} \quad (1)$$

where the symbol 'K_{WT}' and 'T_{WT}' represent the gain and the time constants of the WT generator, respectively.

2.2. The Mathematical Model of Solar–Thermal Power Generation

Solar power generation plays a significant role as an eco-friendly and carbon-neutral electricity source in modern power systems. This renewable energy is efficiently harnessed using solar panels or heat-exchanging systems. It is worth noting that the transfer function of the solar–thermal power plant system can be represented as a linear function, described by the specific form given in Equation (2) as demonstrated by [28].

$$G_s(s) = \frac{K_s}{1 + sT_s} \frac{K_T}{1 + sT_T} = \frac{\Delta P_{STPG}}{\Delta P_{solar}} \quad (2)$$

In Equation (2), the variables 'K_s' and 'K_T' represent the gain constants, while the time constants of the solar–thermal power plant are denoted by the terms 'T_s' and 'T_T'.

2.3. The Mathematical Model of Fuel Cell and Electrolyzer

Fuel cells operate as electrochemical energy conversion devices in which hydrogen and oxygen react to produce electricity, with water being the primary by-product. It holds immense importance in modern power grids and has gained widespread recognition due to its notable benefits, including high efficiency and minimal environmental impact [18]. Despite the presence of various nonlinear elements, the behavior of a fuel cell can be effectively approximated by a first-order linear model, as represented by Equation (3).

$$G_{FC}(s) = \frac{K_{FC}}{1 + sT_{FC}} \quad (3)$$

In the aforementioned equation, K_{FC} and T_{FC} correspond to the gain and the time constants of the fuel cell, respectively.

The aqua electrolyzer has the essential function of providing hydrogen to the fuel cell, harnessing a fraction of the electrical energy generated from wind and solar power sources [18]. In this process, a proportion of $(1 - K_n)$ of the wind and PV energy is employed for water electrolysis, thus contributing to the production of hydrogen used in fuel cells. To simplify its representation, the aqua electrolyzer model can be depicted using a first-order transfer function, as illustrated in [29].

$$G_{AE}(s) = \frac{K_{AE}}{1 + sT_{AE}} = \frac{\Delta P_{AE}}{(\Delta P_{WTPG} + \Delta P_{STPG})(1 - K_n)} \quad (4)$$

In this relationship, it is assumed that K_n is determined by the equation that $K_n = \frac{P_t}{(P_{WTPG} + P_{STPG})}$, where its value in the simulation is considered 0.6. The gain and time constants of the electrolyzer are respectively denoted by K_{AE} and T_{AE}. Although first-order linear transfer functions for fuel cells and electrolyzers are widely used in LFC studies, actual electrochemical devices exhibit nonlinear dynamics, especially under fast transients. The linear approximation neglects charge double-layer effects, potentially smoothing high-frequency responses. However, LFC primarily deals with low-frequency oscillations around

the nominal grid frequency, where this simplification is considered acceptable and ensures fair controller comparison.

To conduct a thorough comparison of previous studies, the hybrid power system suggested in [18,24,25] is employed as the test system. The system's specifications, as illustrated in Figure 1, are provided below.

$T_{12} = T_{21} = 0.08674$ p.u.MW/rad.Hz, $K_{psi} = 200$ Hz/(p.u.MW), $T_{psi} = 20$ s, $T_{ri} = 10$ s, $T_{Gi} = 0.08$ s, $T_{ti} = 0.3$ s, $B_i = 0.425$ p.u.MW/Hz, $R_i = 2.4$ p.u.MW/Hz, $D_i = 5.01 \times 10^{-3}$ p.u.MW/Hz, $H_i = 3$ s, $K_s = 1.8$, $T_s = 1.8$ s, $K_T = 1$, $T_T = 0.3$ s, $K_{WT} = 1$, $T_{WT} = 1.5$ s, $K_{AE} = 0.002$, $T_{AE} = 0.5$ s, $K_{FC} = 0.01$, $T_{FC} = 4$ s, $a_{12} = 1$, $K_n = 0.6$.

3. Optimization Through Coot Algorithm

The COA concept, first proposed by [22], is applied to optimizing COA-AFOPID parameters. Inspired by the movement patterns of coots, the COA aims to replicate two specific modes observed in coots' movement on water. The COA follows a series of predetermined steps outlined in [22,30]. To start the population, a random initialization process is used, following the equation provided below.

$$Coot_p(i) = rand(1, d) * (u_{cb} - l_{cb}) + l_{cb} \tag{5}$$

Here, $Coot_p(i)$ represents the positional coordinates of ith coot. The number of decision variables and the boundaries of the search space are denoted by d, u_{cb}, and l_{cb}, respectively.

- The cost function is derived for every coot's position. Additionally, the values of N_L and N_{coot}, representing the number of leaders and coots, respectively, are randomly selected to determine the global optimum, identifying the optimal leader or coot.
- During this step, the coots' positions are modified using four different movements, which are explained as follows.

3.1. The Swarm Undergoes Random Movements in Different Directions

To initiate this process, a random position labeled as Q is generated using the following equation:

$$Q = rand(1, d) * (u_{cb} - l_{cb}) + l_{cb} \tag{6}$$

To avoid the swarm getting stuck in local optima, the position Q is updated using the following equations:

$$A_{coa} = 1 - iter * \left(\frac{1}{maxiter}\right) \tag{7}$$

$$Coot_p(i) = Coot_p(i) + A_{coa} * R_2 * (Q - Coot_p(i)) \tag{8}$$

In the given equation, B_{coa} and R_2 represent variables linked to coot movement and a random number chosen from the interval [0, 1]. Additionally, *iter* and *maxiter* represent the current iteration and the maximum iteration, respectively.

3.2. Chain Movement

To simulate the movement of a chain consisting of two coots, the average position is calculated using Equation (9).

$$Coot_p(i) = 0.5 * (Coot_p(i-1) + Coot_p(i)) \tag{9}$$

3.3. Adjusting the Position Based on the Group Leaders

The coots align themselves with their respective group leaders, thereby adjusting their positions correspondingly. Let K denote the index number of the leader. Furthermore,

i represents the index number of the current coot, and N_L refers to the total number of leaders. The selection of a leader by a coot is described by Equation (10):

$$K = 1 + (i \; MOD \; N_L) \tag{10}$$

The cost function is determined for each coot's position. In the mentioned movement process, the coots' positions are updated according to the following step:

$$Coot_p(i) = Leader_p(K) + 2 * R_1 * cos(2\pi R) * (Leader_p(K) - Coot_p(i)) \tag{11}$$

Here, R_1 represents a randomly chosen value within the range of [0, 1]. Similarly, $Leader_p(k)$ denotes the selected leader positions, while R indicates a random value within the interval of $[-1, 1]$.

In the above equation, R_1 denotes a random value within the range [0, 1]. Moreover, $Leader_p(k)$ and R represent the positions of the selected leader and a randomly selected value within the range $[-1, 1]$, respectively.

3.4. Varying Positions of Group Leaders

The group leader continuously adjusts its position using Equations (12) and (13) to move towards the optimal region and achieve convergence.

$$B_{coa} = 2 - iter * \left(\frac{1}{maxiter}\right) \tag{12}$$

$$Leader_p(i) = \begin{cases} B_{coa} * R_3 * \cos(2\pi R) * \left(gbest - Leader_p(i)\right) \\ \qquad +gbest \quad R_4 < 0.5 \qquad (a) \\ B_{coa} * R_3 * cos(2\pi R) * \left(gbest - Leader_p(i)\right) \\ \qquad -gbest \quad R_4 \geq 0.5 \qquad (b) \end{cases} \tag{13}$$

In the above equations, R_3 and R_4 represent random values within the range [0, 1]. Additionally, $gbest$ refers to the best position discovered thus far, while B_{coa} is a variable related to the movement of the leader.

- Continue iterating steps iii to iv of the algorithm until the stop condition is met. As the number of iterations grows, the algorithm progressively approaches the optimal cost function and ultimately achieves convergence.

The effectiveness of the COA in optimizing controller parameters has been validated in several recent studies. El-Bahay et al. applied COA to tune FOPID controllers for load frequency control in a two-area power system and demonstrated its superiority over particle swarm optimization (PSO), water cycle algorithm, atomic orbital search, and honey badger algorithm. Similarly, the COA has been successfully employed for optimal tuning of PID controllers in power systems with renewable energy sources and electric vehicles, achieving significant improvement in transient response specifications compared to other algorithms [31]. Furthermore, comparative studies on other engineering problems have confirmed that COA outperforms both PSO and genetic algorithm (GA) [30,31]. These findings collectively support the selection of COA as the optimization algorithm for tuning the proposed AFOPID controller in this study. Therefore, only the results obtained with the COA-optimized controller are presented in the following sections.

4. The Proposed LFC Controller

4.1. The Coa-Based PID and FOPID Controllers

Fractional calculus, a field within mathematics, introduces the concept of non-integer order derivatives and integrals. It utilizes the fundamental operator, denoted as ${}_aD_t^\alpha$, as defined in Equation (14), to generalize the order of derivatives and integrals of non-integer values.

$$ {}_aD_t^\alpha = \begin{cases} \frac{d^\alpha}{dt^\alpha} & \alpha > 0 \\ 1 & \alpha = 0 \\ \int_a^t (d\tau)^\alpha & \alpha < 0 \end{cases} \tag{14} $$

In this formulation, α denotes the operation order, and a represents the initial condition of the system, where α belongs to the set of real numbers ($\alpha \in R$). To mathematically formulate non-integer integro-differential relationships, researchers typically rely on several established frameworks, including the Caputo, Riemann–Liouville, and Grünwald–Letnikov definitions. Among these, Caputo's formula is the commonly used approximation method [32,33], defined by the following equation.

$$ D^\alpha f(t) = \frac{1}{\Gamma(m-\alpha)} \int_0^t \frac{D^m f(t)}{(t-\tau)^{\alpha+1-m}} d\tau, \alpha \in R^+, \quad m \in Z^+, m-1 \le \alpha \le m \tag{15} $$

In this equation, α represents the derivative order of f(t) with all initial states set to zero, while $\Gamma(\,)$ denotes the Gamma function. The Laplace transform corresponding to the Caputo fractional-order derivative can be written as

$$ L\{{}_aD_t^\alpha\} = \int_0^\infty e^{-st} D^\alpha f(t) dt = s^\alpha F(s) - \sum_{k=0}^{m-1} s^{\alpha-k-1} D^k f(0) \tag{16} $$

Here, $L\{\cdot\}$ is the Laplace operator. The formulation of the fractional-order differential function presents a considerable challenge when compared to the integer-order differential function. To address this difficulty, certain approximation and numerical techniques have been suggested [34]. A reduced-complexity approximation scheme for non-integer operators, leveraging a continuous pole-zero distribution was originally presented in [34]. This algorithm involves constructing an integer-order transfer function through the recursive distribution of N poles and N zeroes within a frequency interval $[\omega_l, \omega_h]$ for N corner frequencies [34,35]. The mathematical representation of this approximation is defined by Equation (17).

$$ s^\alpha \approx k \prod_{n=1}^{N} \frac{1 + \frac{s}{\omega_{z,n}}}{1 + \frac{s}{\omega_{p,n}}}, \alpha > 0 \tag{17} $$

The parameter k, as the adjusted gain, is utilized to calibrate both sides of Equation (17) so that the gain at 1 rad/s is equal to unity. The initial application of fractional-order controllers in dynamic control systems was documented by [34]. A comparative study conducted by this study demonstrated the superior performance of these controllers compared to classical PID controllers. Subsequently, ref. [12] introduced a generalized form of the PID controller, referred to as FOPID. Figure 2 illustrates the block diagram depicting the COA-PID and COA-FOPID controllers.

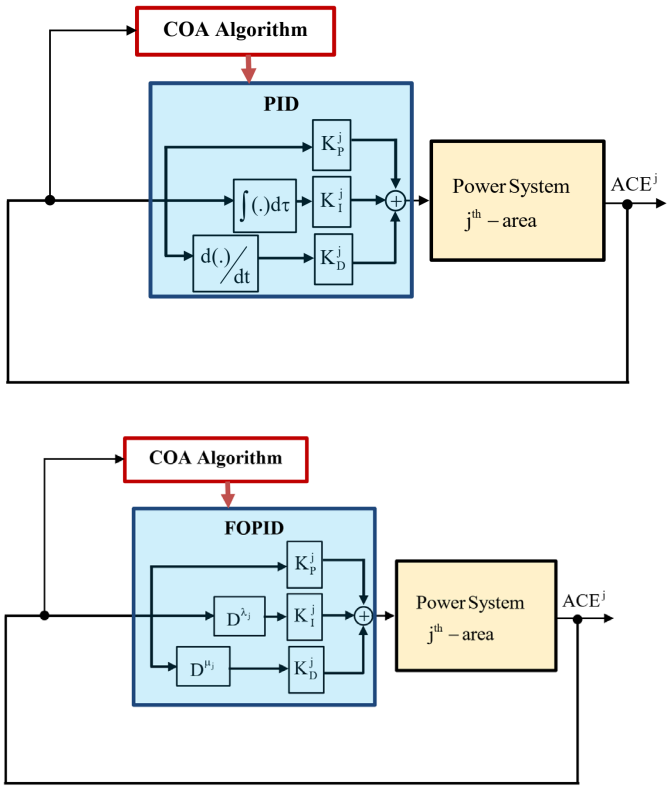


Figure 2. Comparative Block Diagrams of COA-PID and COA-FOPID Control Architectures.

The transfer functions of a PID controller and a FOPID controller can be expressed using the following equations:

$$u_{COA-PID_j}(t) = K_P^j ACE_j(t) + K_I^j \int_0^t ACE_j(\tau)d\tau + K_D^j \frac{dACE_j(t)}{dt} \tag{18}$$

$$u_{COA-FOPID_j}(t) = K_P^j ACE_j(t) + K_I^j D^{-\lambda_j} ACE_j(t) + K_D^j D^{\mu_j} ACE_j(t) \tag{19}$$

In this equation, K_P^j, K_I^j, K_D^j, $\lambda_j > 0$, and $\mu_j > 0$ represent the proportional gain, integral gain, derivative gains, integral order, and derivative order, respectively. Comparing it to the PID controller, the FOPID controller possesses a more intricate design structure. It introduces two extra tuning parameters (integral and derivative orders) compared to the PID controller. However, these additional parameters offer greater flexibility in the design process, allowing for the achievement of optimal performance criteria.

Several cost functions have been proposed for the optimal design of controllers in the LFC field [7,14]. In this study, the cost function $F_c(\chi_D)$ is employed for the optimization of the proposed control structure, as defined in Equation (20):

$$F_c(\chi_D) = \int_{t=0}^{t=T_{sim}} t.(|\Delta f_1| + |\Delta f_2| + |\Delta p_{tie}|)dt \tag{20}$$

The design process of the proposed controller involves defining specific intervals for the controller parameters. The intervals for the parameter values are considered as follows: $0 < K_P^j \leq 10$, $0 < K_I^j \leq 10$, $0 < K_D^j \leq 10$, $0 < \lambda^j \leq 1$, and $0 < \mu^j \leq 1$, respectively.

4.2. The Proposed COA Based Adaptive Fractional Order PID LFC Controller

The predetermined values of FOPID controller parameters limit the controller's ability to effectively compensate for uncertainties in system parameters and environmental disturbances. Finding an optimal set of K_P, K_I, K_D, λ, and μ that ensures robust control

performance under all operating conditions is challenging. The fixed fractional-order parameters in FOPID controllers reduce adaptability, leading to suboptimal performance during transient disturbances and unnecessary control effort in steady-state conditions. This issue is particularly prominent in LFC systems that experience sudden changes in system states, rendering the FOPID control approach inefficient.

By selecting appropriate values for λ and μ based on the error condition, the proposed FOPID control law can be transformed into an integer order P, PI, PD, or PID controller, as depicted in Figure 3 [36]. The distinct categories of integer-order mechanisms are tailored to manage distinct stages of the operational cycle. Specifically, when facing sudden network shifts or cold starts, employing a restrained integral action alongside a strengthened derivative response is highly beneficial for suppressing peak deviations and accelerating the return to stability. On the other hand, as the system response approaches the steady state, it is preferable to have a stiffer integral control effort and a softer derivative control effort to ensure smooth settling with minimum fluctuations. Achieving this arrangement requires dynamically tuning the values of λ and μ through an online feedback-driven adaptation framework using state and error information. This scheme enables a seamless transition of fractional orders between 0 and 1, allowing for a smooth adjustment of the control behavior [36].

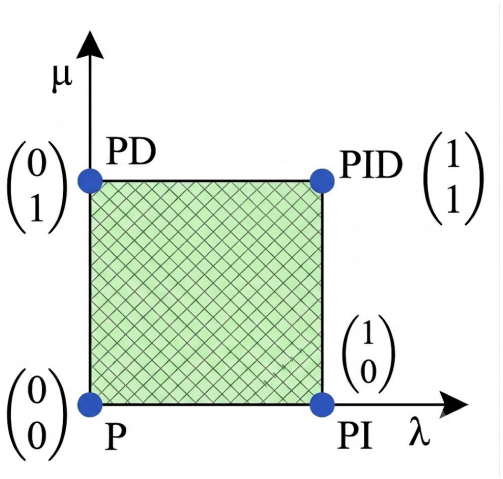


Figure 3. Expansion of point to the plane in FOPID controller.

This scheme removes the need for offline pre-calibration of the fractional orders λ and μ. The adaptation strategy is governed by rules based on state error. During transient conditions, when the system deviates significantly from the reference, λ is reduced while μ is increased. This increases the derivative action and improves the speed of the transient response.

As the response approaches the reference, λ is gradually increased while μ is decreased. This adjustment enhances the integral action, effectively reducing overshoot and oscillations, and enabling smooth convergence to the reference value. For practical implementation, a pre-calibrated hyperbolic secant function (HSF) is employed within the adaptation scheme.

The HSF is mathematically adopted from [23,37], which applied it to DC motor speed control. In the present work, the HSF is for the first time adapted to multi-area load frequency control by defining the compounded error variable based on the area control error (ACE). The HSF depends on a weighted sum of the error $ACE(t)$ and its derivative $\dot{ACE}(t)$. The HSF is chosen for its smooth waveform, ensuring a smooth transition of parameters, its bounded range between 0 and 1, and its even symmetry. These characteristics align with

the aforementioned meta-rules. The time-varying functions used for online self-adaptation of the fractional orders λ and μ are defined in Equations (21) and (22).

$$\lambda(t) = sech(z(t)) \tag{21}$$

$$\mu(t) = 1 - \lambda(t) \tag{22}$$

The compounded error variable, $z(t)$ is defined as $z(t) = \beta ACE(t) + \delta \dot{ACE}(t)$, where β and δ are preconfigured positive constants determining the variation rate of the HSF, and $sech(.)$ represents the HSF. The optimal values of β and δ are calculated using the tuning procedure discussed in the next section. These two parameters play a crucial role in configuring the shape and form of the HSF. The compounded error variable $z(t)$, obtained from the weighted sum of $ACE(t)$ and $\dot{ACE}(t)$, provides accurate information about the phase of the system's state response. When the response deviates further from the desired reference, the compounded error variable automatically increases, as depicted in Figure 4, leading to an increase in μ and a decrease in λ using the adaptation functions described in Equations (21) and (22). Similarly, as the response converges to the desired reference, the magnitude of the compounded error decreases, as shown in Figure 4, resulting in a decrease in μ and an increase in λ. This arrangement fully aligns with the previously mentioned rules. By incorporating the self-adjusting fractional orders, the resulting Adaptive-FOPID (A-FOPID) control law can be expressed as given in Equation (23).

$$u_{COA-AFOPID_i}(t) = K_P^j ACE_j(t) + K_I^j D^{-\lambda_j(t)} ACE_j(t) + K_D^j D^{\mu_j(t)} ACE_j(t) \tag{23}$$

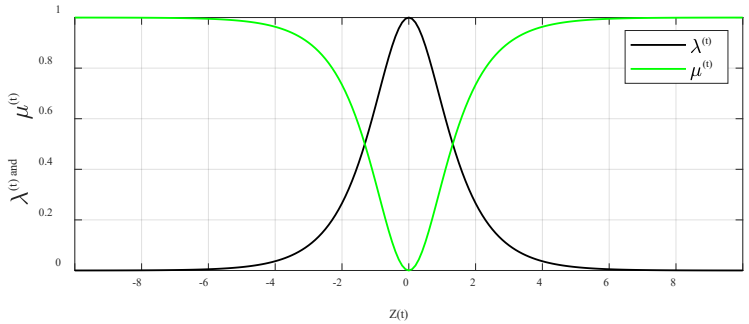


Figure 4. Waveform Analysis of HSFs for Fractional Order Self-Adjustment.

The COA-AFOPID control law requires the re-calibration of the parameters K_P, K_I, K_D, λ, and μ, which can be achieved by utilizing the tuning procedure detailed in Section 4. The functions $\lambda(t)$ and $\mu(t)$ can be straightforwardly programmed in the simulation software. Solving these algebraic equations can be done in a single step following each sampling instant, ensuring that there is no recursive computational burden on the digital computer. The block diagram of the COA-AFOPID control system is illustrated in Figure 5.

Using the cost function defined in Equation (17), the following interval is considered for the constant parameters of the proposed COA-AFOPID controller.

$0 < K_P^j \leq 10$, $0 < K_I^j \leq 10$, $0 < K_D^j \leq 10$, $0 < \beta^j \leq 1$, and $0 < \delta^j \leq 1$, respectively.

The computational cost of the proposed controller was evaluated on a standard desktop platform. The execution time per sampling step is well below the typical control signal update period in practical LFC systems. Therefore, the proposed COA-AFOPID strategy meets the real-time requirements of practical grid frequency scheduling.

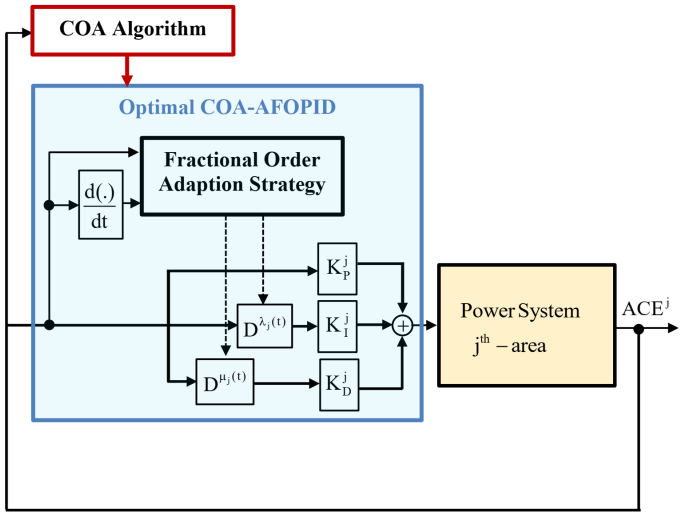


Figure 5. Block diagram of the proposed COA-AFOPID control system.

5. Simulation Results

To evaluate the effectiveness of the COA-AFOPID controllers that have been developed, a series of comprehensive simulations are carried out using the system model outlined in Section 2. The COA is employed with a designated swarm size, $N_{max} = 100$, and a predetermined number of iterations, $K_{max} = 50$. The results obtained from applying the COA to the COA-based PI, PID, FOPID, and COA-AFOPID controllers are presented in Table 2.

Table 2. Parameters of the designed COA-based PI, PID, FOPID, and AFOPID controllers for the power system under evaluation.

	K_P	K_I	K_D	λ	μ	β	δ
COA-PI	1.132	2.192	-	-	-	-	-
COA-PID	1.982	3.105	0.937	-	-	-	-
COA-FOPID	2.854	2.364	1.108	0.842	0.671	-	-
COA-AFOPID	3.015	3.672	1.682	-	-	0.087	0.031

The COA-based AFOPID controller updates the FOPID parameters at each time step. Its performance is assessed across four scenarios, and compared against COA-based PI, PID, and FOPID controllers. The system parameters relevant to this analysis are available in Section 2, and specific values like 50% load, GRC of 0.03 p.u.MW/min and GDB of 0.05 have been taken into account for the analysis [18,24,25,27,29].

5.1. First Scenario: Investigation of the Effect of Changes in Large Loads

Scenario 1 investigates a comprehensive model of a modern power system. It is important to note that the two-zone grid considered in this study has identical parameters, but they are modified due to a load step change. In Zone 1, the factory's capacity shifts to 0.025 per unit, while in Zone 2, it changes to 0.015 per unit. The dynamic responses of frequency deviation and tie-line power flow for this specific scenario are illustrated in Figures 6–9. Moreover, Figure 10 displays variations in the values of λ, μ and control efforts.

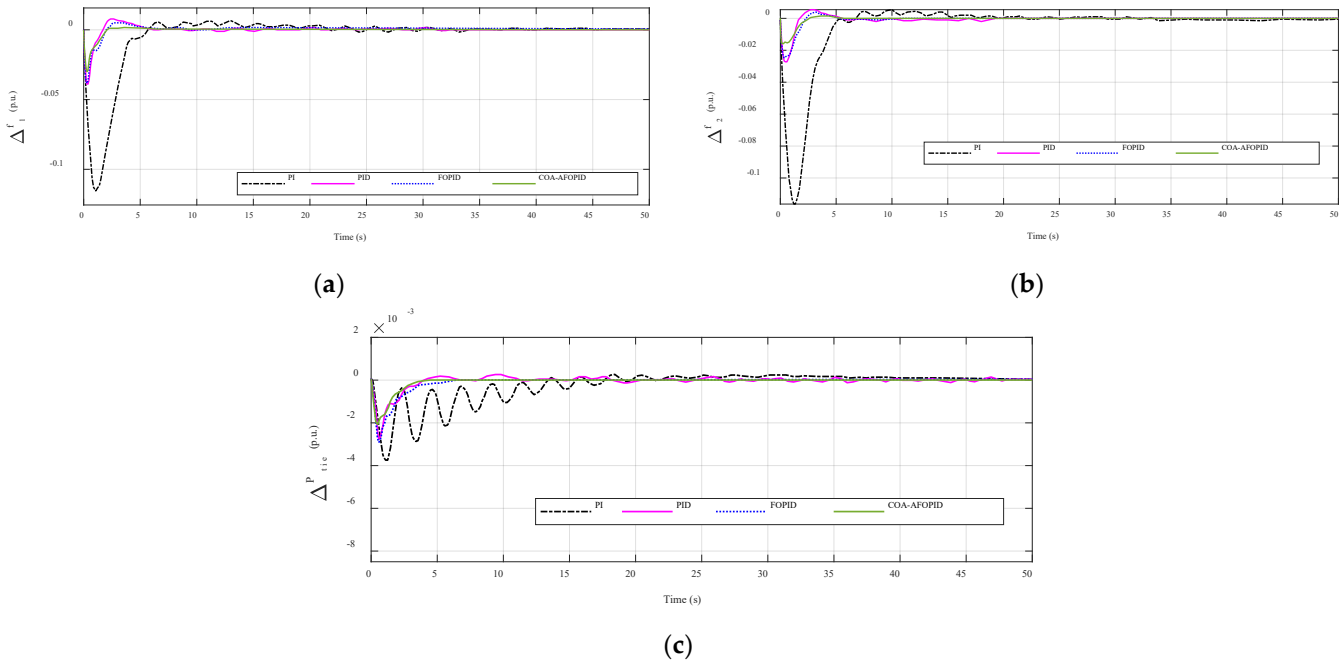


Figure 6. Dynamic responses of (**a**) Δf_1 (**b**) Δf_2 and (**c**) P_{tie} for the first scenario.

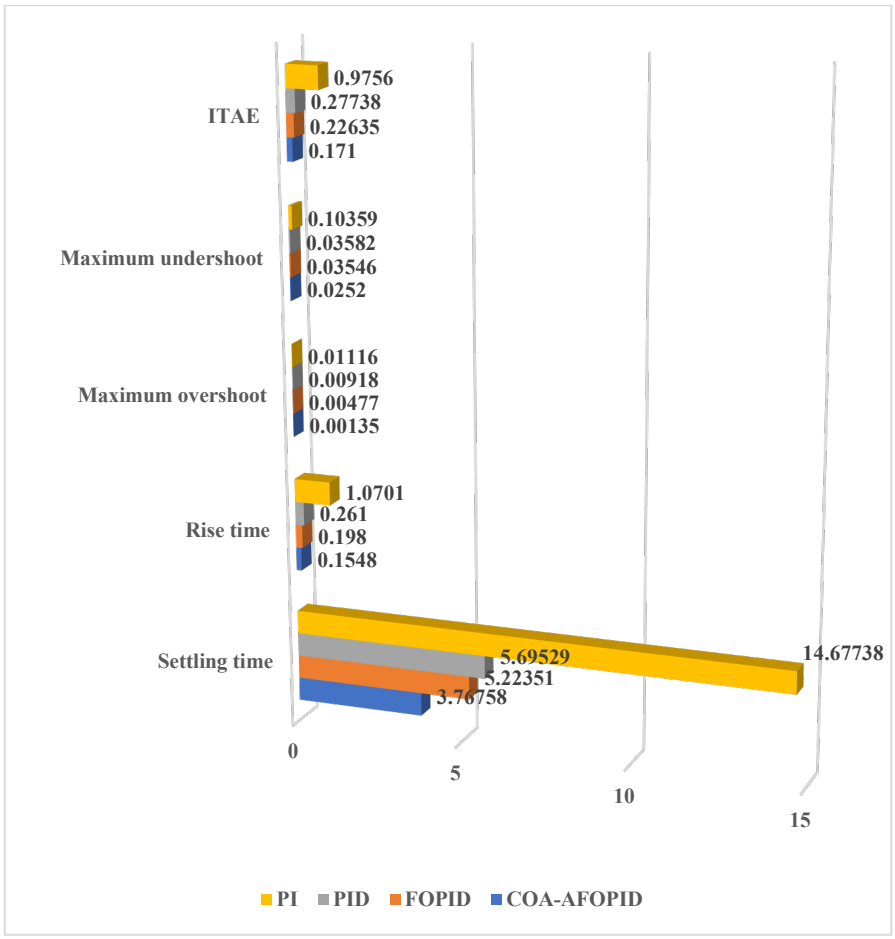


Figure 7. Performance indices of Δf_1 for the first scenario.

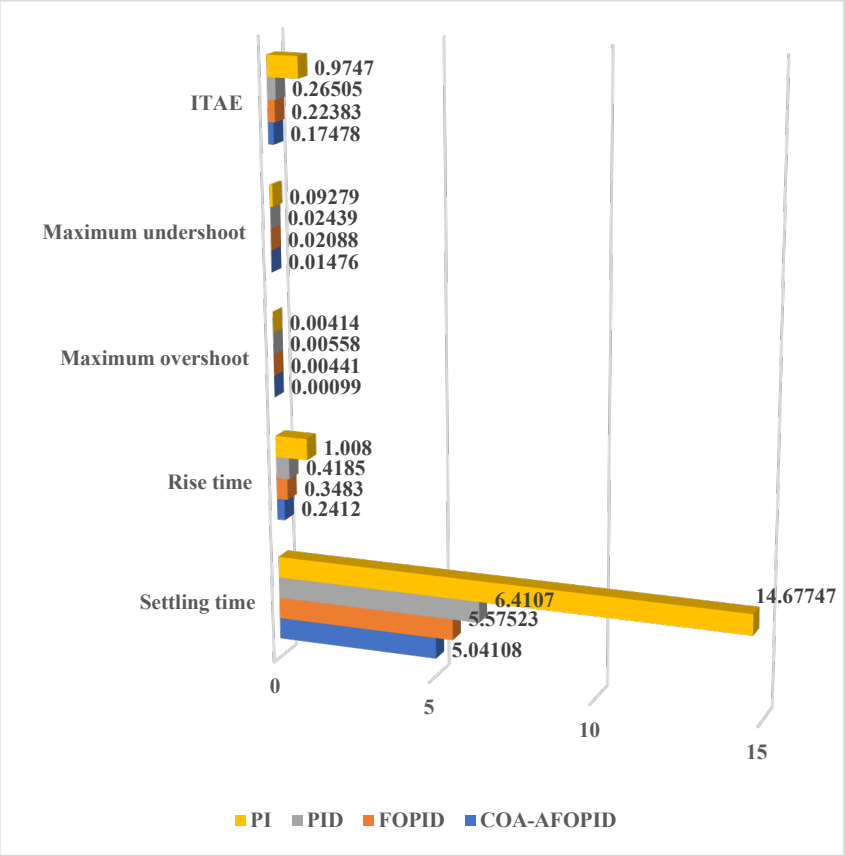


Figure 8. Performance indices of Δf_2 for the first scenario.

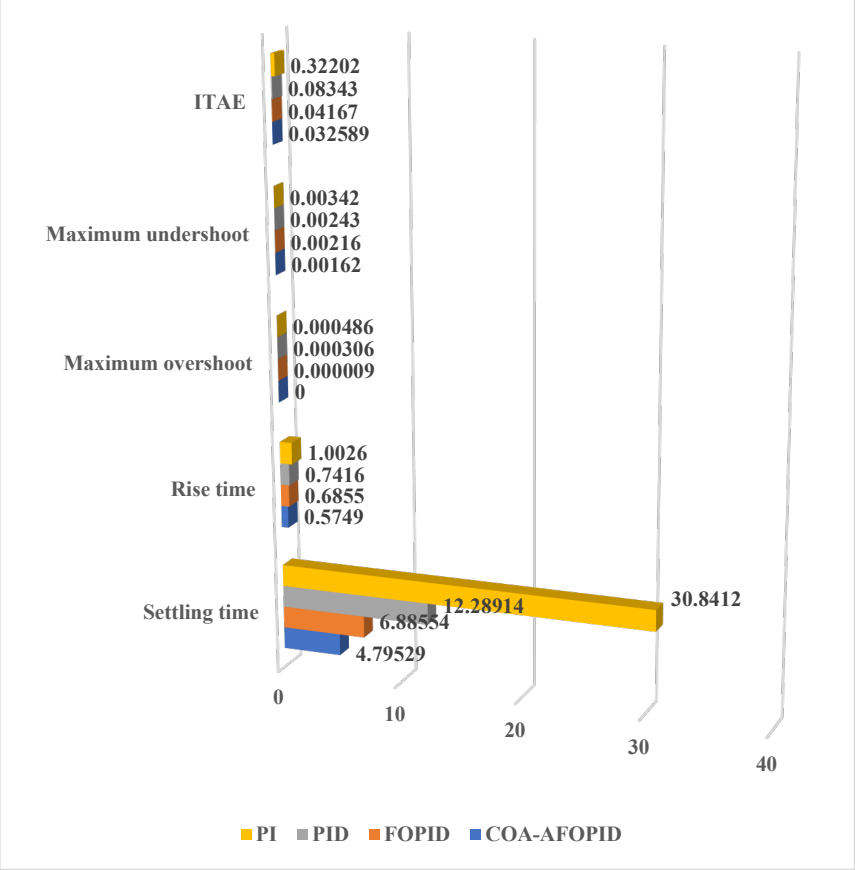
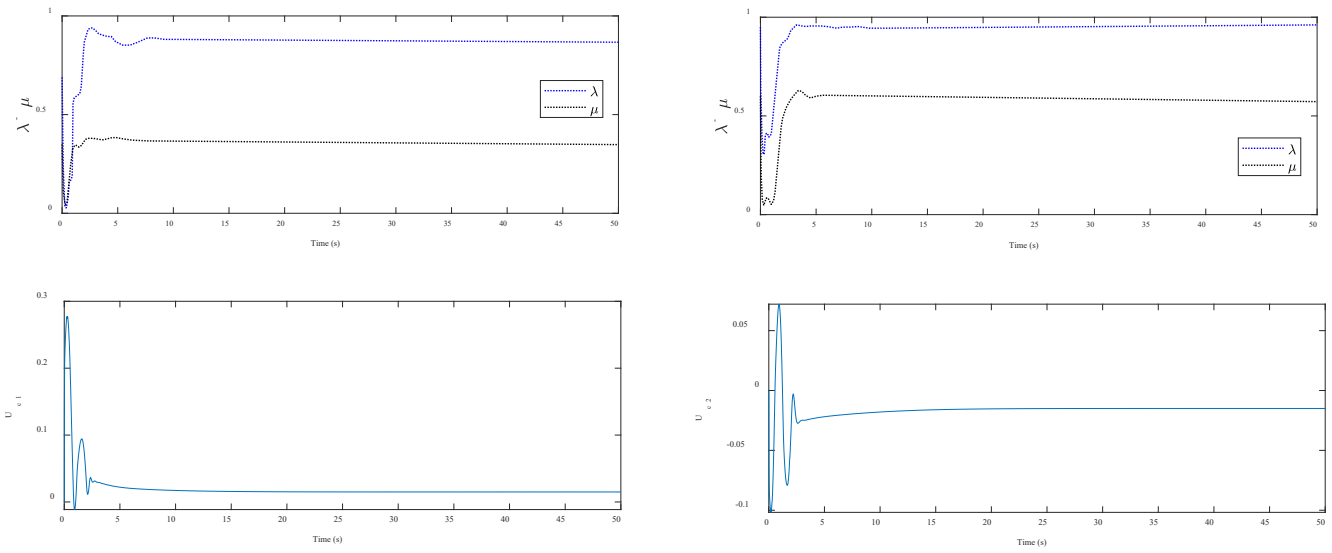


Figure 9. Performance indices of ΔP_{tie} for the first scenario.



(**a**) (**b**)

Figure 10. The variations of λ, μ and control efforts for (**a**) region-1 and (**b**) region-2.

From Figures 6–9, it becomes evident that the proposed COA-AFOPID controller effectively reduces performance metrics when compared to PI, PID, and FOPID controllers. When comparing the COA-AFOPID controller with the other controllers under study, it is evident that the COA-AFOPID controller outperforms the others across various metrics. As shown in Figure 10, the control efforts for both region-1 and region-2 remain well below the typical actuator saturation limits. Moreover, the control signals exhibit smooth and continuous variations without high-frequency oscillations or abrupt jumps. This behavior confirms that the proposed COA-AFOPID controller, despite its adaptive nature, does not cause excessive mechanical wear or actuator saturation.

5.1.1. Comparing Results of Δf_1 for the First Scenario

Considering Δf_1 response for the first scenario, in terms of settling time, the COA-AFOPID controller achieves a much lower value of 3.76758, representing an improvement of approximately 46.06% compared to FOPID (5.22351), 33.84% compared to PID (5.69529), and 74.38% compared to PI (14.67738). Similarly, the COA-AFOPID controller demonstrates faster rise time, with a percentage improvement of approximately 22.73% compared to FOPID (0.198), 40.92% compared to PID (0.261), and 85.51% compared to PI (1.0701). Furthermore, for the ITAE metric, the COA-AFOPID controller achieves an ITAE value of 0.171, showcasing notable improvements of approximately 24.54% compared to FOPID (0.22635), 38.39% compared to PID (0.27738), and 82.48% compared to PI (0.9756).

5.1.2. Comparing Results of Δf_2 for the First Scenario

In terms of Δf_2 for the first scenario, the COA-AFOPID controller achieves significant improvements in settling time with a value of 5.04108, representing approximately 9.59% improvement compared to FOPID (5.57523), 21.16% improvement compared to PID (6.4107), and 65.62% improvement compared to PI (14.67747). Additionally, the COA-AFOPID controller exhibits a faster rise time with a percentage improvement of approximately 30.8% compared to FOPID (0.3483), 42.48% compared to PID (0.4185), and 76.08% compared to PI (1.008). Furthermore, the COA-AFOPID controller showcases an ITAE value of 0.17478, indicating improvements of approximately 21.86% compared to FOPID (0.22383), 34.01% compared to PID (0.26505), and 82.03% compared to PI (0.9747).

5.1.3. Comparing Results of ΔP_{tie} for the First Scenario

In terms of ΔP_{tie}, the COA-AFOPID controller achieves a significantly lower settling time of 4.79529, indicating an improvement of approximately 30.57% compared to FOPID (6.88554), 60.96% compared to PID (12.28914), and 84.45% compared to PI (30.8412). In terms of rise time, the COA-AFOPID controller demonstrates a faster response, showcasing a percentage improvement of about 16.13% compared to FOPID (0.6855), 22.48% compared to PID (0.7416), and 42.66% compared to PI (1.0026). Additionally, for the ITAE metric, the COA-AFOPID controller showcases a significantly lower value of 0.032589, representing an improvement of approximately 21.26% compared to FOPID (0.04167), 60.93% compared to PID (0.08343), and 89.89% compared to PI (0.32202).

In this scenario, the COA-AFOPID controller demonstrates enhanced performance across various metrics, specifically achieving lower settling time, faster rise time, minimal overshoot and undershoot, and reduced ITAE compared to the other controllers. These results highlight the superior performance and effectiveness of the COA-AFOPID controller in load frequency control applications.

5.2. Second Scenario: Investigation of the Effect of Residential Load

The second scenario shares similarities with the first scenario in terms of conditions. Both zones experience step load fluctuations, resulting in a generation relationship (23). Figures 11–14 present detailed information on the dynamic responses of frequency deviation and tie power flow fluctuations. Additionally, Figure 15 demonstrates variations in the values of λ, μ and control efforts, which are essential control parameters.

$$P_S = P_{Thermal} + P_{Wind} + P_{Solar} - P_{AE} + P_{FC} \quad (24)$$

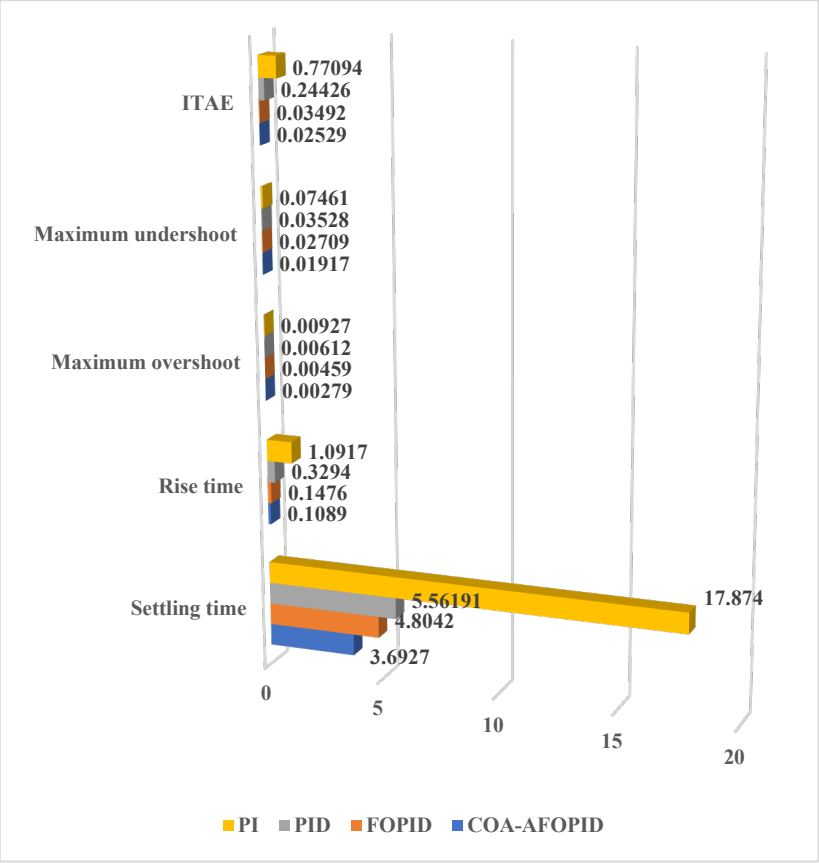


Figure 11. Performance indices of Δf_1 for the second scenario.

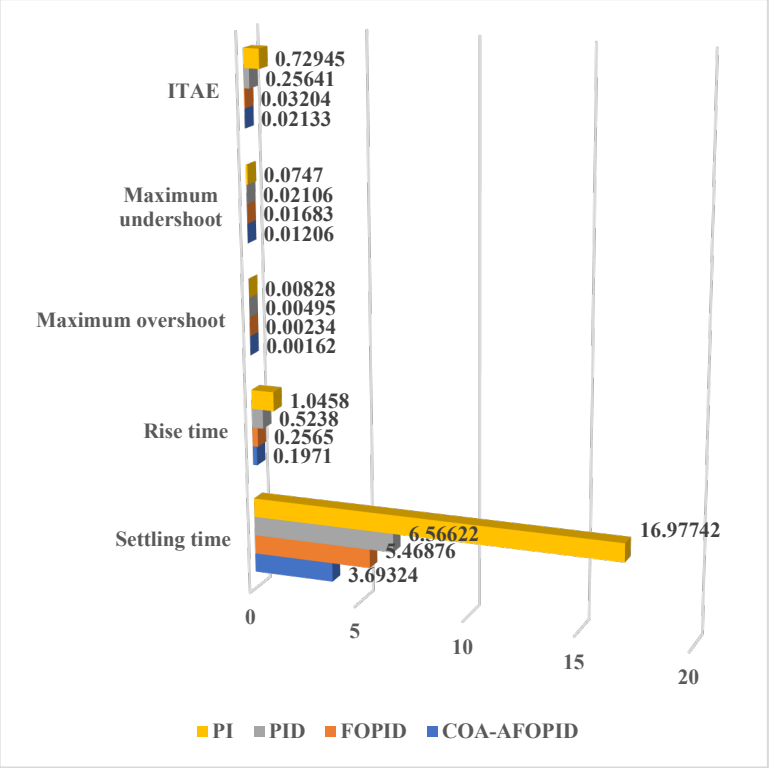


Figure 12. Performance indices of Δf_2 for the second scenario.

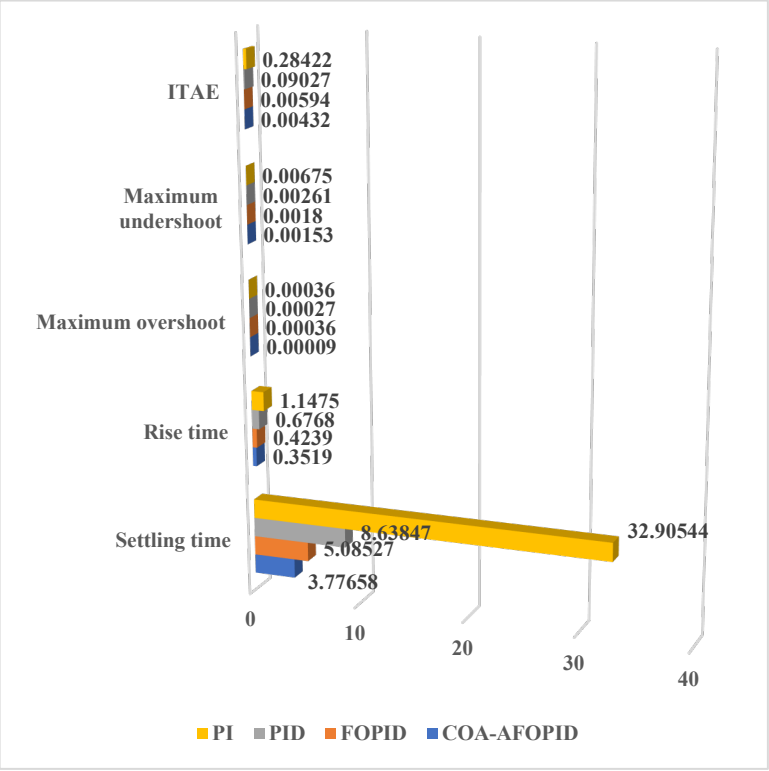
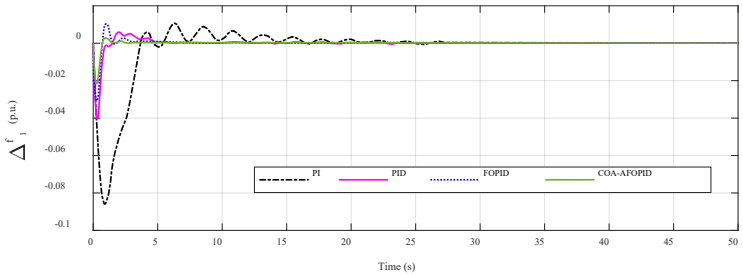
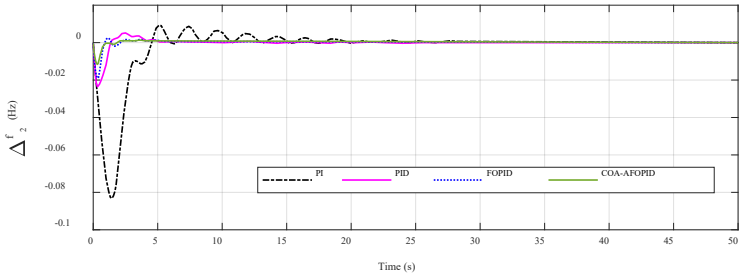


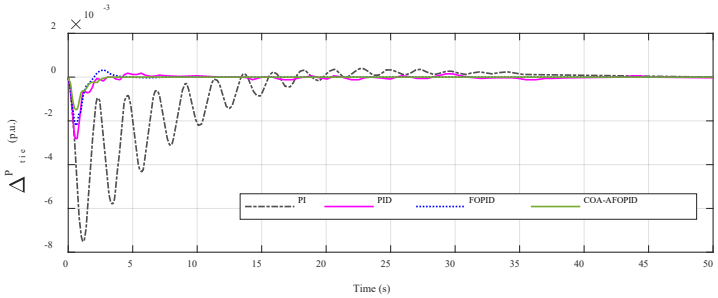
Figure 13. Performance indices of ΔP_{tie} for the second scenario.



(**a**)

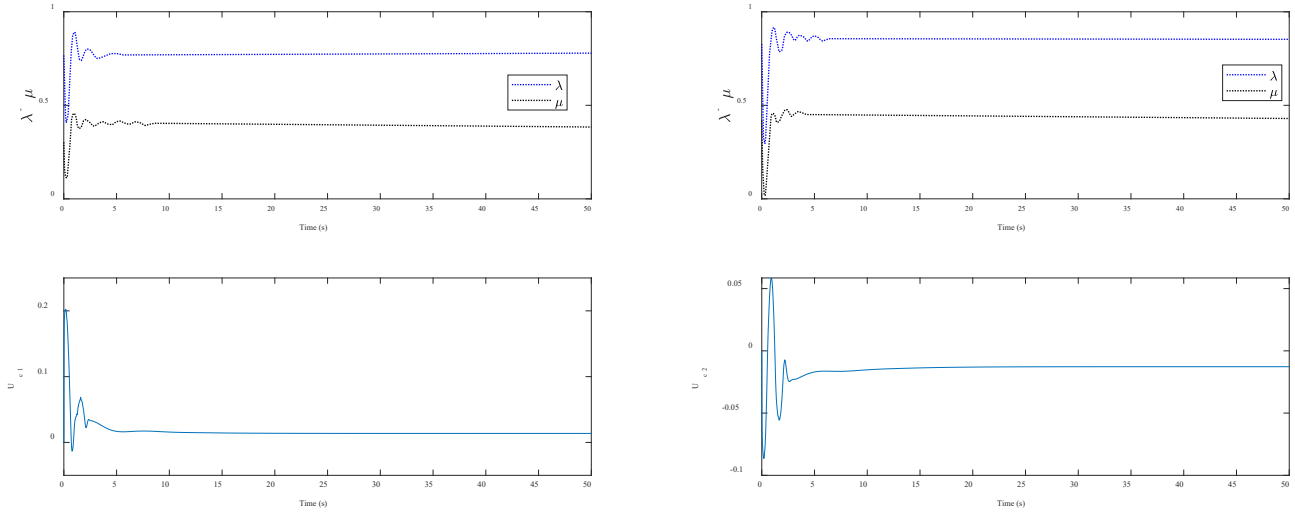


(**b**)



(**c**)

Figure 14. Dynamic Response Comparison of Variables (**a**) Δf_1, (**b**) Δf_2 and (**c**) P_{tie} for the second scenario.



(**a**) (**b**)

Figure 15. The variations of λ, μ and control efforts for (**a**) region-1 and (**b**) region-2.

In this scenario, the COA-AFOPID controller demonstrates superior performance compared to the other controllers across multiple performance indices. Similar to the

first scenario, the control effort waveforms presented in Figure 15 for the second scenario demonstrate that the proposed controller respects the physical limitations imposed by GRC and GDB. The control signals are smooth, bounded, and free from chattering, even under residential load variations. These observations further support the practical viability of the proposed COA-AFOPID strategy for real-time frequency regulation applications without risk of actuator damage or excessive maintenance requirements.

5.2.1. Comparing Results of Δf_1 for the Second Scenario

The COA-AFOPID controller achieves a significantly lower settling time of 3.6927, indicating an improvement of approximately 22.94% compared to FOPID (4.8042), 33.59% compared to PID (5.56191), and 79.34% compared to PI (17.874). In terms of rise time, the COA-AFOPID controller demonstrates a faster response, showcasing a percentage improvement of about 26.17% compared to FOPID (0.1476), 67.03% compared to PID (0.3294), and 90.04% compared to PI (1.0917). Additionally, for the ITAE metric, the COA-AFOPID controller showcases a remarkably lower value of 0.02529, representing an improvement of approximately 27.64% compared to FOPID (0.03492), 89.63% compared to PID (0.24426), and 96.70% compared to PI (0.77094).

5.2.2. Comparing Results of Δf_2 for the Second Scenario

Compared to the FOPID, PID, and PI controllers across different metrics, the COA-AFOPID controller achieves a substantially lower settling time of 3.69324, indicating an improvement of approximately 32.45% compared to FOPID (5.46876), 43.77% compared to PID (6.56622), and 78.25% compared to PI (16.97742). Additionally, the COA-AFOPID controller exhibits a faster response in terms of rise time, with a percentage improvement of about 23.27% compared to FOPID (0.2565), 62.37% compared to PID (0.5238), and 81.17% compared to PI (1.0458). Furthermore, the COA-AFOPID controller achieves a significantly lower value of 0.02133 for the ITAE metric, representing an improvement of approximately 33.43% compared to FOPID (0.03204), 91.68% compared to PID (0.25641), and 97.07% compared to PI (0.72945).

5.2.3. Comparing Results of ΔP_{tie} for the Second Scenario

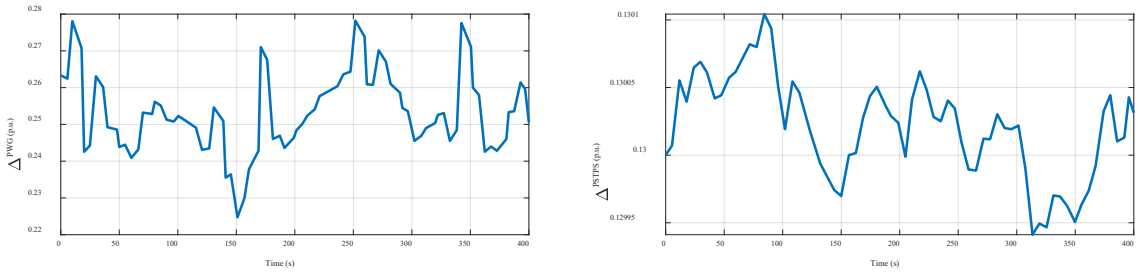
In terms of ΔP_{tie}, the COA-AFOPID controller demonstrates remarkable improvements in settling time compared to the FOPID, PID, and PI controllers. It achieves a substantially lower settling time of 3.77658, representing an improvement of approximately 25.75% compared to FOPID (5.08527), 56.32% compared to PID (8.63847), and 88.53% compared to PI (32.90544). Moreover, the COA-AFOPID controller exhibits a faster response in terms of rise time, with a percentage improvement of approximately 17.06% compared to FOPID (0.4239), 48.01% compared to PID (0.6768), and 69.30% compared to PI (1.1475). Furthermore, for the ITAE metric, the COA-AFOPID controller achieves a significantly lower value of 0.00432, representing an improvement of approximately 27.34% compared to FOPID (0.00594), 95.21% compared to PID (0.09027), and 98.47% compared to PI (0.28422).

These results establish the superiority of the COA-AFOPID controller, demonstrating significant improvements in settling time, rise time, maximum overshoot, undershoot, and overall control performance when compared to the PID family and FOPID control mechanisms.

5.3. Third Scenario: Investigation of the Effect of Stochastic RESS Generation

This scenario investigates the effectiveness of the designed control mechanism regarding the effect of RESs on the power grid being studied. The unpredictable nature of electricity generation from wind turbines and solar–thermal sources requires careful analysis. To address this issue, stochastic fluctuations in the power output from RESs as well as

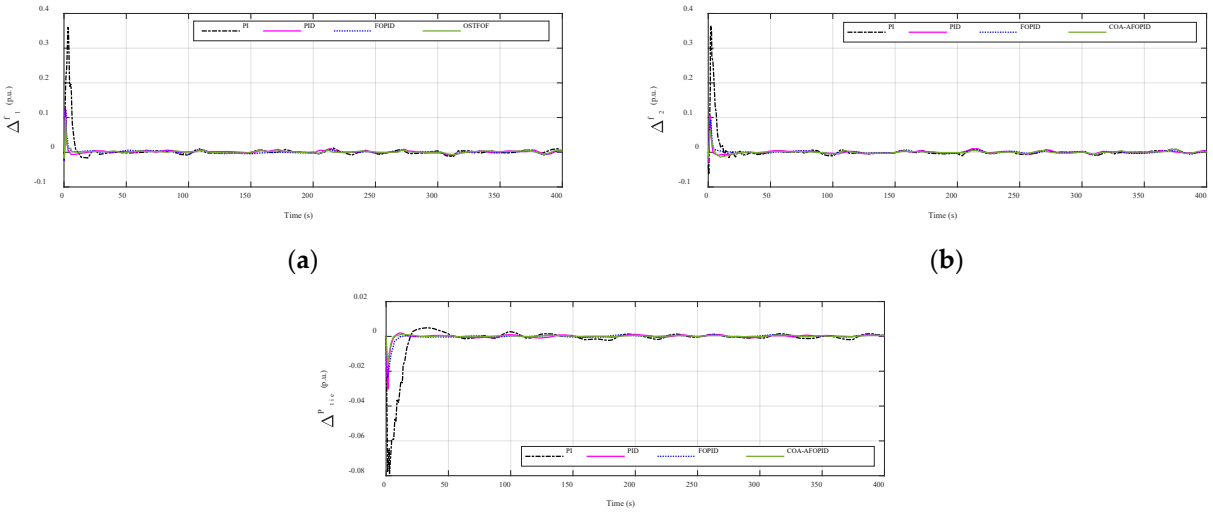
random load disturbances are introduced to the hybrid power system. Figure 16 depicts the stochastic characteristics of the fluctuations in wind generation and the solar–thermal plant.



(**a**) (**b**)

Figure 16. Stochastic variation in output power for (**a**) wind and (**b**) solar thermal generation.

The dynamic responses of frequency variation and tie power flow changes are illustrated in Figures 17 and 18. In comparison to the PID family, and FOPID control mechanisms, these figures demonstrate that the max undershoot was remarkably reduced, which was achieved through the implementation of the proposed COA-AFOPID controller. In the scenario where wind and solar–thermal generation undergo random fluctuations, the IAE index values associated with the PI, PID, and COA-AFOPID controllers are presented in Table 3, specifically in parts (a) and (b). When analyzing the information provided in Table 3 and referring to Figures 17 and 18, it becomes apparent that the COA-AFOPID controller demonstrates minimal response fluctuations when faced with random variations in wind generator and solar–thermal power system outputs.



(**a**) (**b**)

(**c**)

Figure 17. Dynamic responses of (**a**) Δf_1, (**b**) Δf_2 and (**c**) P_{tie} related to the third scenario for changes in wind power generation.

For instance, in the case of the Δf_1 response to the random output power changes in wind generators, and in terms of the IAE metric, the COA-AFOPID controller outperforms the PI, PID, and FOPID controllers, achieving up to 22.33% improvement over PID and 64.99% improvement over PI. It achieves significant improvements of about 17.01%, 21.42%, and 64.22% over FOPID, PID, and PI controllers in the Δf_2, and approximately 25.29%, 35.11%, and 85.49% improvements over FOPID, PID, and PI controllers in the ΔP_{tie}.

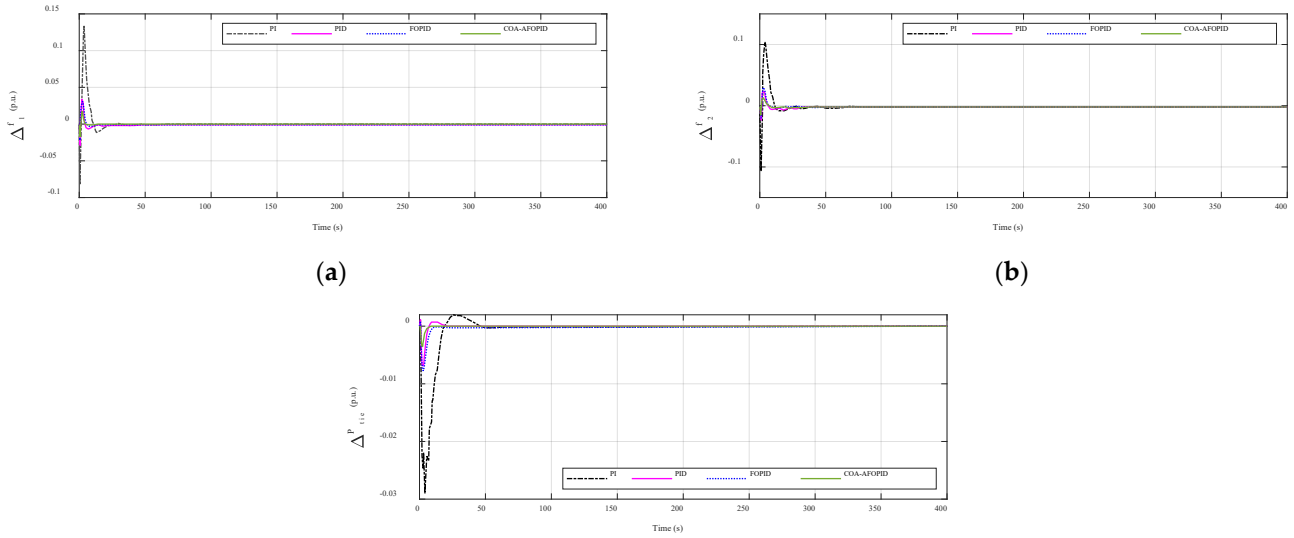


Figure 18. Dynamic responses of (**a**) Δf_1, (**b**) Δf_2 and (**c**) P_{tie} related to the third scenario for changes in solar thermal power generation.

Table 3. Performance evaluation based on the IAE index related to the third scenario.

		PI	PID	FOPID	COA-AFOPID
(a)	Δf_1	2.90272	1.30754	1.16184	1.01614
	Δf_2	2.7213	1.20508	1.14492	0.95034
	ΔP_{tie}	1.06878	0.2397	0.20774	0.1551
(b)	Δf_1	0.70876	0.36942	0.32336	0.24534
	Δf_2	0.66082	0.3431	0.27354	0.24816
	ΔP_{tie}	0.27918	0.08084	0.06768	0.04606

5.4. Fourth Scenario: Investigation of the Effect of Arbitrary Variations in Load Demand

The final scenario is dedicated to investigating the impact of arbitrary load demand variations. The random changes in load demand considered in this study are visually presented in Figure 19. The dynamic responses, specifically concerning frequency deviation and tie power flow changes, concerning this scenario, are illustrated in Figure 20.

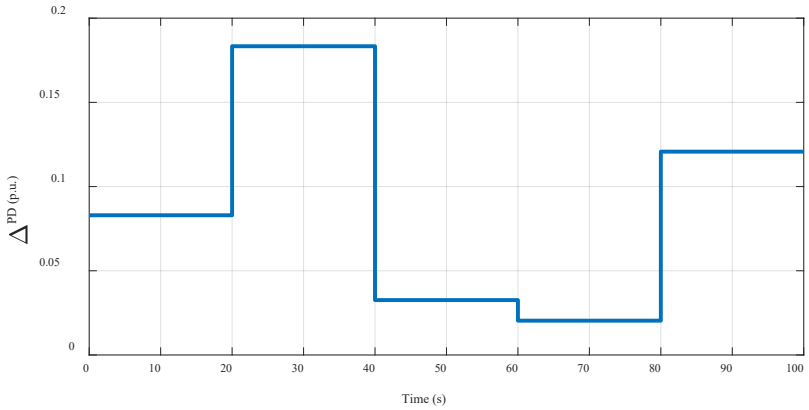


Figure 19. Arbitrary variations in load for the fourth scenario.

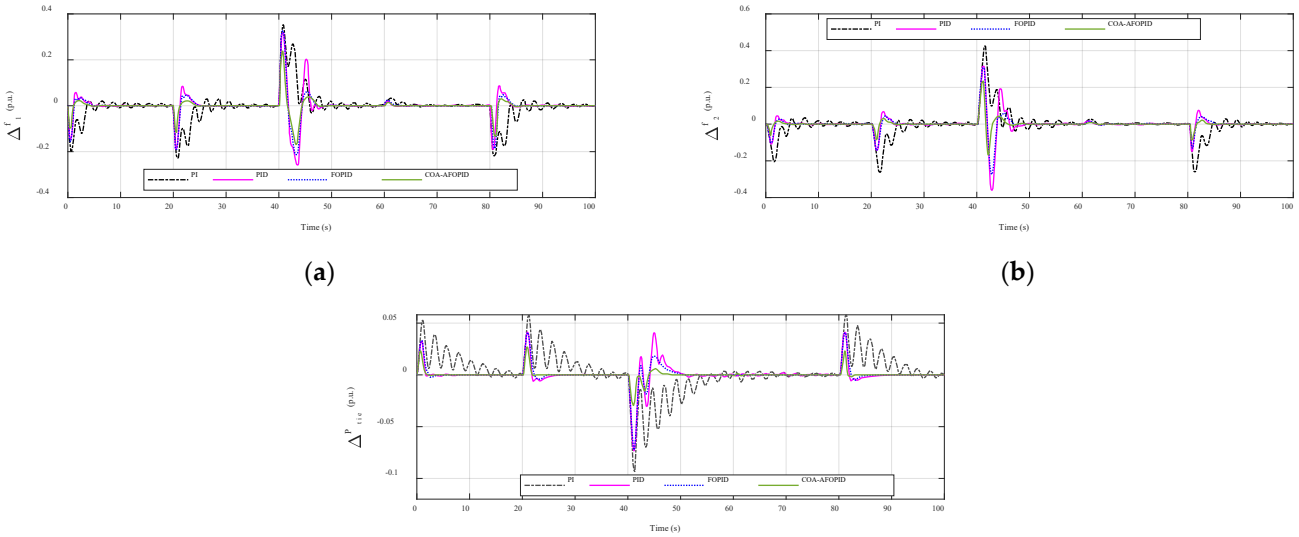


Figure 20. Dynamic responses of (**a**) Δf_1, (**b**) Δf_2 and (**c**) P_{tie} related to the fourth scenario.

To quantitatively investigate the grid's performance in response to random load variations, the IAE index values for the COA-AFOPID controller are compared to those of the PI, PID, and FOPID controllers, as presented in Table 4. By analyzing the outcomes of the final scenario, as depicted in Figure 20 and described in Table 4, it becomes apparent that the COA-AFOPID controller significantly improves the system's behavior compared to the responses of the PI, PID, and FOPID controllers, particularly in the presence of random load variations. Notably, the COA-AFOPID controller achieves a notable reduction in maximum fluctuations and enhances the dynamic behavior of the system.

Table 4. Performance evaluation based on IAE related to the fourth scenario.

	PI	PID	FOPID	COA-AFOPID
Δf_1	5.78664	2.06706	1.50024	0.95128
Δf_2	4.92278	1.92136	1.17218	0.78114
ΔP_{tie}	1.0434	0.3008	0.20304	0.14382

To assess the system's performance in the presence of random load variations, the IAE (Integral of Absolute Error) index values of Δf_1 response and Δf_2 response were analyzed for the COA-AFOPID, PI, PID, and FOPID controllers. The COA-AFOPID controller demonstrates superior performance with lower IAE index values of 0.95128 and 0.78114 compared to FOPID (1.50024 and 1.17218), PID (2.06706 and 1.92136), and PI (5.78664 and 4.92278) controllers, respectively. These IAE index values represent percentage improvements of approximately 36.50% and 32.53% over FOPID, 53.95% and 41.93% over PID, and an impressive 83.52% and 84.11% over PI.

In this scenario, the COA-AFOPID control strategy demonstrates superior performance over the PI, PID, and FOPID control strategies considering the IAE index values, showcasing significant improvements ranging from 32.53% to 84.11% over the other three controllers. These results highlight the superiority of the COA-AFOPID controller in dealing with random load variations.

5.5. Robustness Analysis Under Parameter Perturbations

To evaluate the robustness of the proposed COA-AFOPID controller against internal system parameter uncertainties, a sensitivity analysis was conducted by varying the inertia

constant H and damping factor D by ±25% from their nominal values. These parameters are selected because they significantly influence frequency response dynamics. The simulation was performed under the step load disturbance described in Scenario 1. Table 5 summarizes the performance indices for Δf_1 response under nominal and perturbed conditions.

Table 5. Robustness analysis of the proposed COA-AFOPID controller under ±25% parameter variations (Scenario 1-Δf_1 response).

Parameter	Variation	Settling Time (s)	ITAE	Overshoot (p.u.)	Undershoot (p.u.)
Nominal	0%	3.7676	0.171	0.00135	0.0252
H (Inertia)	25%	3.82	0.174	0.00137	0.0255
	−25%	3.92	0.18	0.00142	0.026
D (Damping)	25%	3.68	0.165	0.00132	0.0248
	−25%	3.95	0.184	0.00145	0.0265

As shown in Table 5, the proposed controller maintains excellent performance under all perturbed conditions. The maximum degradation in ITAE is only 7.6% (for −25% variation in D), while the maximum change in settling time is 4.8%. All performance variations remain well below 10%, confirming that the proposed COA-AFOPID controller exhibits strong robustness against parameter uncertainties. This characteristic is essential for practical power system applications where exact parameter values are often uncertain or time-varying.

6. Conclusions

In this paper, an adaptive fractional-order PID (AFOPID) controller optimized by the Coot Optimization Algorithm (COA) was proposed for load frequency control (LFC) of a modern hybrid power system incorporating thermal power plants, wind farms, solar–thermal generation, electrolyzers, and fuel cells. The proposed COA-AFOPID controller features real-time adjustment of fractional orders λ and μ using a hyperbolic secant function (HSF), enabling adaptive responses to varying operating conditions. Nonlinear physical constraints including generation rate constraints and governor dead band were considered in the system model. The performance of the proposed controller was comprehensively evaluated under four distinct scenarios and benchmarked against PI, PID, and conventional FOPID controllers.

The main findings and contributions of this study are summarized as follows:

- The proposed COA-AFOPID controller consistently outperformed PI, PID, and conventional FOPID controllers across all four scenarios in terms of settling time, rise time, overshoot/undershoot reduction, and ITAE index.
- For the Δf_1 response, the COA-AFOPID controller achieved a settling time improvement of 46.06% compared to FOPID, 33.84% compared to PID, and 74.38% compared to PI. ITAE index improvements reached 24.54%, 38.39%, and 82.48%, respectively.
- Under residential load variations, the proposed controller demonstrated ITAE improvements of 27.64% over FOPID, 89.63% over PID, and 96.70% over PI for the Δf_1 response.
- The COA-AFOPID controller effectively handled random fluctuations in wind and solar–thermal power outputs, achieving IAE improvements of up to 22.33% over PID and 64.99% over PI.
- Under random load demand changes, the proposed controller achieved IAE improvements ranging from 32.53% to 84.11% compared to PI, PID, and FOPID controllers.

- The real-time self-tuning of fractional orders λ and μ based on the hyperbolic secant function proved highly effective, allowing the controller to transition between integer-order and fractional-order behaviors according to the system's transient and steady-state conditions.

In summary, the proposed COA-AFOPID controller offers a robust, adaptive, and high-performance solution for load frequency control in modern power systems with high penetration of renewable energy sources. The results confirm its superiority over conventional PI, PID, and fixed-parameter FOPID controllers, making it a promising candidate for frequency regulation in sustainable energy networks.

Author Contributions: Conceptualization: D.B., A.B., and K.Y.; methodology: S.S. and K.Y.; writing—original draft preparation: Y.M. and K.Y.; formal analysis: D.B. and M.S.; validation: Y.M. and S.S.; funding acquisition: D.B. and S.S.; and writing—review and editing: A.B. and M.S. All authors have read and agreed to the published version of the manuscript.

Funding: This research was funded by the Committee of Science of the Ministry of Science and Higher Education of the Republic of Kazakhstan (grant no.BR24992964).

Data Availability Statement: All data generated or analyzed during this study are included in this published article.

Conflicts of Interest: The authors have no relevant conflicts of interest to disclose.

References

1. Sahoo, G.; Sahu, R.K.; Panda, S.; Samal, N.R.; Arya, Y. Modified Harris Hawks Optimization-Based Fractional-Order Fuzzy PID Controller for Frequency Regulation of Multi-Micro-Grid. *Arab. J. Sci. Eng.* **2023**, *48*, 14381–14405.
2. Saxena, A.; Shankar, R. Improved Load Frequency Control Considering Dynamic Demand Regulated Power System Integrating Renewable Sources and Hybrid Energy Storage System. *Sustain. Energy Technol. Assess.* **2022**, *52*, 102245. [CrossRef]
3. Khan, I.A.; Mokhlis, H.; Mansor, N.N.; Illias, H.A.; Awalin, L.J.; Wang, L. New Trends and Future Directions in Load Frequency Control and Flexible Power System: A Comprehensive Review. *Alex. Eng. J.* **2023**, *71*, 263–308. [CrossRef]
4. Liu, Y.; Chen, Y.; Li, M. Dynamic Event-Based Model Predictive Load Frequency Control for Power Systems under Cyber Attacks. *IEEE Trans. Smart Grid* **2021**, *12*, 715–725.
5. Lu, K.; Zhou, W.; Zeng, G.; Zheng, Y. Constrained Population Extremal Optimization-Based Robust Load Frequency Control of Multi-Area Interconnected Power System. *Int. J. Electr. Power Energy Syst.* **2019**, *105*, 249–271.
6. Mir, A.S.; Senroy, N. Adaptive Model Predictive Control Scheme for Application of SMES for Load Frequency Control. *IEEE Trans. Power Syst.* **2017**, *32*, 4756–4765.
7. Padhi, J.R.; Debnath, M.K.; Kar, S.K. Self-Tuning Fuzzy-PI Controller for Load Frequency Control Analysis with the Integration of Wind Energy. *Energy Sources Part A Recovery Util. Environ. Eff.* **2022**, *44*, 613–631.
8. Onyeka, A.E.; Yan, X.-G.; Mao, Z.; Jiang, B.; Zhang, Q. Robust Decentralised Load Frequency Control for Interconnected Time Delay Power Systems Using Sliding Mode Techniques. *IET Control Theory Appl.* **2020**, *14*, 470–480. [CrossRef]
9. Sobhy, M.A.; Abdelaziz, A.Y.; Hasanien, H.M.; Ezzat, M. Marine Predators Algorithm for Load Frequency Control of Modern Interconnected Power Systems Including Renewable Energy Sources and Energy Storage Units. *Ain Shams Eng. J.* **2021**, *12*, 3843–3857. [CrossRef]
10. Mohamed, T.H.; Alamin, M.A.M.; Hassan, A.M. A Novel Adaptive Load Frequency Control in Single and Interconnected Power Systems. *Ain Shams Eng. J.* **2021**, *12*, 1763–1773. [CrossRef]
11. Zamani, A.; Barakati, S.M.; Yousofi-Darmian, S. Design of a Fractional Order PID Controller Using GBMO Algorithm for Load-Frequency Control with Governor Saturation Consideration. *ISA Trans.* **2016**, *64*, 56–66. [PubMed]
12. Podlubny, I. Fractional-Order Systems and PIλDμ-Controllers. *IEEE Trans. Autom. Control* **1999**, *44*, 208–214.
13. Asgari, S.; Suratgar, A.A.; Kazemi, M. Feedforward Fractional Order PID Load Frequency Control of Microgrid Using Harmony Search Algorithm. *Iran. J. Sci. Technol. Trans. Electr. Eng.* **2021**, *45*, 1369–1381. [CrossRef]
14. Zamani, A.-A.; Shafiee, M.; Sajadinia, M. Optimal Self-Tuning Fractional Order Fuzzy Load Frequency Control Considering Sustainable Energy Sources and Electric Vehicle. *Int. J. Ambient Energy* **2023**, *44*, 2170–2184. [CrossRef]
15. Fathy, A.; Yousri, D.; Rezk, H.; Thanikanti, S.B.; Hasanien, H.M. A Robust Fractional-Order PID Controller Based Load Frequency Control Using Modified Hunger Games Search Optimizer. *Energy* **2022**, *15*, 361. [CrossRef]

16. Pahadasingh, S.; Jena, C.; Panigrahi, C.K. Load Frequency Control Incorporating Electric Vehicles Using FOPID Controller with HVDC Link. In *Innovation in Electrical Power Engineering, Communication, and Computing Technology: Proceedings of IEPCCT 2019*; Springer: Singapore, 2020; pp. 181–203.
17. Latif, A.; Hussain, S.M.S.; Das, D.C.; Ustun, T.S.; Iqbal, A. A Review on Fractional Order (FO) Controllers' Optimization for Load Frequency Stabilization in Power Networks. *Energy Rep.* **2021**, *7*, 4009–4021. [CrossRef]
18. Irudayaraj, A.X.R.; Wahab, N.I.A.; Umamaheswari, M.G.; Radzi, M.A.M.; Sulaiman, N.B.; Veerasamy, V.; Prasanna, S.C.; Ramachandran, R. A Matignon's Theorem Based Stability Analysis of Hybrid Power System for Automatic Load Frequency Control Using Atom Search Optimized FOPID Controller. *IEEE Access* **2020**, *8*, 168751–168772. [CrossRef]
19. Guha, D.; Roy, P.K.; Banerjee, S. Quasi-Oppositional Jaya Optimized 2-Degree-of-Freedom PID Controller for Load-Frequency Control of Interconnected Power Systems. *Int. J. Model. Simul.* **2022**, *42*, 63–85.
20. Nayak, J.R.; Shaw, B.; Sahu, B.K.; Naidu, K.A. Application of Optimized Adaptive Crow Search Algorithm Based Two Degree of Freedom Optimal Fuzzy PID Controller for AGC System. *Eng. Sci. Technol. Int. J.* **2022**, *32*, 101061. [CrossRef]
21. Kundur, P. Power System Stability and Control. In *Power System Stability and Control*; Kundur, P., Ed.; McGraw-Hill: New York, NY, USA, 2007; Volume 10, p. 7-1.
22. Naruei, I.; Keynia, F. A New Optimization Method Based on Coot Bird Natural Life Model. *Expert. Syst. Appl.* **2021**, *183*, 115352. [CrossRef]
23. Saleem, O.; Mahmood-Ul-Hasan, K. Adaptive Collaborative Speed Control of PMDC Motor Using Hyperbolic Secant Functions and Particle Swarm Optimization. *Turk. J. Electr. Eng. Comput. Sci.* **2018**, *26*, 1612–1622. [CrossRef]
24. Kler, D.; Kumar, V.; Rana, K.P.S. Optimal Integral Minus Proportional Derivative Controller Design by Evolutionary Algorithm for Thermal-Renewable Energy-Hybrid Power Systems. *IET Renew. Power Gener.* **2019**, *13*, 2000–2012.
25. Veerasamy, V.; Wahab, N.I.A.; Ramachandran, R.; Vinayagam, A.; Othman, M.L.; Hizam, H.; Satheeshkumar, J. Automatic Load Frequency Control of a Multi-Area Dynamic Interconnected Power System Using a Hybrid PSO-GSA-Tuned PID Controller. *Sustain* **2019**, *11*, 6908.
26. Shafiee, M.; Zamani, A.-A.; Sajadinia, M. Using Improved DDAO Algorithm to Solve Economic Emission Load Dispatch Problem in the Presence of Wind Farms. *Int. J. Ind. Electron. Control Optim.* **2023**, *6*, 161–169.
27. Pahasa, J.; Ngamroo, I. Coordinated Control of Wind Turbine Blade Pitch Angle and PHEVs Using MPCs for Load Frequency Control of Microgrid. *IEEE Syst. J.* **2016**, *10*, 97–105.
28. Kumar, R.; Sinha, N. Modeling and Control of Dish-Stirling Solar Thermal Integrated with PMDC Generator Optimized by Meta-Heuristic Approach. *IEEE Access* **2020**, *8*, 26343–26355.
29. Masuta, T.; Yokoyama, A. Supplementary Load Frequency Control by Use of a Number of Both Electric Vehicles and Heat Pump Water Heaters. *IEEE Trans. Smart Grid* **2012**, *3*, 1253–1262. [CrossRef]
30. Memarzadeh, G.; Keynia, F. A New Optimal Energy Storage System Model for Wind Power Producers Based on Long Short Term Memory and Coot Bird Search Algorithm. *J. Energy Storage* **2021**, *44*, 103401. [CrossRef]
31. El-Bahay, M.H.; Lotfy, M.E.; El-Hameed, M.A. Effective Participation of Wind Turbines in Frequency Control of a Two-Area Power System Using Coot Optimization. *Prot. Control Mod. Power Syst.* **2023**, *8*, 1–15. [CrossRef]
32. Aguila-Camacho, N.; Duarte-Mermoud, M.A. Fractional Adaptive Control for an Automatic Voltage Regulator. *ISA Trans.* **2013**, *52*, 807–815. [CrossRef] [PubMed]
33. Zamani, A.-A.; Etedali, S. Optimal Fractional-Order PID Control Design for Time-Delayed Multi-Input Multi-Output Seismic-Excited Structural System. *J. Vib. Control* **2023**, *29*, 802–819.
34. Oustaloup, A.; Levron, F.; Mathieu, B.; Nanot, F.M. Frequency-Band Complex Noninteger Differentiator: Characterization and Synthesis. *IEEE Trans. Circuits Syst. I Fundam. Theory Appl.* **2000**, *47*, 25–39. [CrossRef]
35. Arya, Y. A Novel CFFOPI-FOPID Controller for AGC Performance Enhancement of Single and Multi-Area Electric Power Systems. *ISA Trans.* **2020**, *100*, 126–135. [PubMed]
36. Zamani, A.-A.; Tavakoli, S.; Etedali, S. Fractional Order PID Control Design for Semi-Active Control of Smart Base-Isolated Structures: A Multi-Objective Cuckoo Search Approach. *ISA Trans.* **2017**, *67*, 222–232. [PubMed]
37. Saleem, O.; Ali, S.; Iqbal, J. Robust MPPT Control of Stand-Alone Photovoltaic Systems via Adaptive Self-Adjusting Fractional Order PID Controller. *Energy* **2023**, *16*, 5039.

Disclaimer/Publisher's Note: The statements, opinions and data contained in all publications are solely those of the individual author(s) and contributor(s) and not of MDPI and/or the editor(s). MDPI and/or the editor(s) disclaim responsibility for any injury to people or property resulting from any ideas, methods, instructions or products referred to in the content.